

Variation of magnetic properties of $\text{Sr}_2\text{FeMoO}_6$ due to oxygen vacancies

Martin Hoffmann¹, Victor N. Antonov,^{2,3} Lev V. Bekenov,^{2,4} Kalevi Kokko,^{5,6} Wolfram Hergert,⁷ and Arthur Ernst^{1,4}

¹Institute for Theoretical Physics, Johannes Kepler University Linz, Altenberger Straße 69, 4040 Linz, Austria

²G. V. Kurdyumov Institute for Metal Physics of the N.A.S. of Ukraine, 36 Vernadsky Street, 03142 Kiev, Ukraine

³Faculty of Mathematics and Informatics, University of Białystok, K. Ciolkowskiego 1M, PL-15-245 Białystok, Poland

⁴Max Planck Institute of Microstructure Physics, Weinberg 2, 06120 Halle, Germany

⁵Department of Physics and Astronomy, University of Turku, FIN-20014 Turku, Finland

⁶Turku University Centre for Materials and Surfaces (MatSurf), Turku, Finland

⁷Institute of Physics, Martin Luther University Halle-Wittenberg, Von-Seckendorff-Platz 1, 06120 Halle, Germany

E-mail: martin.hoffmann@jku.at

Abstract. Oxygen vacancies can be of utmost importance for improving or deteriorating physical properties of oxide materials. Here, we studied from first-principles the electronic and magnetic properties of oxygen vacancies in the double perovskite $\text{Sr}_2\text{FeMoO}_6$ (SFMO). We show that oxygen vacancies can increase the Curie temperature in SFMO, although the total magnetic moment is reduced at the same time. We found also that the experimentally observed valence change of the Fe ions from 3+ to 2+ in the x-ray magnetic circular dichroism (XMCD) measurements is better explained by oxygen vacancies than by the assumed mixed valence state. The agreement of the calculated x-ray absorption spectra and XMCD results with experimental data is considerably improved by inclusion of oxygen vacancies.

1. Introduction

Double perovskites $A_2BB'O_6$ (A = alkaline earth or rare earth metal atoms and BB' = heterovalent transition metal atoms such as $B = \text{Fe, Cr, Mn, Co, Ni}$; $B' = \text{Mo, Re, W}$) often demonstrate intrinsically complex magnetic structures and a wide variety of physical properties (see [1] for a review article on these materials). In order to understand the complex properties, experiments on SFMO included numerous methods like photoemission spectroscopy (PES) [2–4], Mössbauer spectroscopy [5, 6], neutron scattering [7–9], x-ray absorption spectroscopy (XAS), and x-ray magnetic circular dichroism (XMCD) measurements [10–12]. Since the XAS and XMCD spectroscopy is very sensitive to the electronic structure and the local environment, comparing calculated spectra to the available experimental results can provide important information about the chemical composition, the ionic valency, and the degree of electronic correlations in the system. Thus, we simulated the XAS and XMCD spectra with our method and found a better agreement than previous density functional calculations [13]. Our results indicate as well a mixed valency of the Fe ion (Fe^{2+} or Fe^{3+}) observed by experiments [6, 7, 10, 11], but we can also conclude from our study that the mixed valency is mainly caused by oxygen vacancies.

In addition, several experimental and theoretical studies have demonstrated that the double perovskite system $\text{Sr}_2\text{FeMoO}_6$ (SFMO) and other related materials exhibit a ferrimagnetic (FiM) half-metallic ground state with a high Curie temperature of 324 K to 420 K [14–17]. The physical origin of the magnetoresistance in SFMO is half-metallicity [18], i.e., the material is an insulator in one of the spin channels, but a metal in the other. This leads to a complete spin polarization at the Fermi level, which immediately suggests their application as a source of spin polarized charge carriers in spintronic devices. Therein, SFMO will be used mainly as a thin film, and many attempts were made to grown high quality films [16, 17, 19–21]. But all these films yield a reduced Curie temperature, which is up to 80 K smaller than for bulk samples [16, 17]. Even for bulk SFMO the theoretical magnetic moment of $4 \mu_B$ was rarely experimentally observed [8]. Such variations were attributed to lattice defects like grain boundaries or point defects. In particular, swapping of Fe and Mo ions, antisite disorder (ASD), [22–28] and oxygen vacancies (V_O) [25, 26, 29, 30] were shown to reduce the

magnetization of SFMO.

Nevertheless, no study addressed explicitly the variation of the Curie temperature, T_C , with oxygen vacancies (V_O). We deploy therefore the Korringa-Kohn-Rostoker Green’s function (KKR-GF) method with the coherent potential approximation (CPA). We calculated magnetic coupling constants using the magnetic force theorem [31] and used it with a classical Heisenberg model in order to calculate the Curie temperature similarly done as in Refs. [32, 33]. A similar approach handling ASD from first-principles was beyond the scope of this work, since the distribution of those antisite defects has to be studied carefully. A simple random distribution might be ruled out by Ref. [34] showing a tendency for antiphase patches, which makes the study of the magnetic coupling of antisite defects a work on its own.

In the following section, we describe the lattice structure of SFMO used in our calculations and give details about the calculation techniques. In Sec. 3, we present the XAS and XMCD calculations for the SFMO compound and demonstrate that oxygen vacancies have to be present in SFMO samples. The influence of oxygen vacancies on the electronic structure and magnetic properties is then discussed in Sec. 4.

2. Numerical Details

For our calculations of SFMO, we adopted the experimentally found double perovskite structure, where the oxygen atoms provide an octahedral environment around the Fe and Mo sites. The FeO_6 and MoO_6 octahedra alternate along the three cubic axes, while the Sr atoms occupy the hollow site formed by the corners of the FeO_6 and MoO_6 octahedra at the body-centered positions (figure 1).

SFMO was found to be cubic ($Fm\bar{3}m$) in the paramagnetic phase, but changes into a tetragonal-type structure below a critical temperature [9]. The Sr atoms occupy the $4d$ Wyckoff positions $(0, 1/2, 1/4)$. The Fe atoms occupy the $2a$ Wyckoff pos. $(0, 0, 0)$ and Mo the $4d$ Wyckoff pos. $(0, 0, 1/2)$. There are two types of oxygen atoms with O_z at the $4e$ Wyckoff pos. $(0, 0, z)$ and O_{xy} at the $8h$ Wyckoff pos. $(x, y, 0)$ (figure 1). Their positions is not definite and varies between different studies. They occupy either the site exactly between Mo and Fe, which gives the body centered tetragonal structure type ($I4/mmm$; No. 139

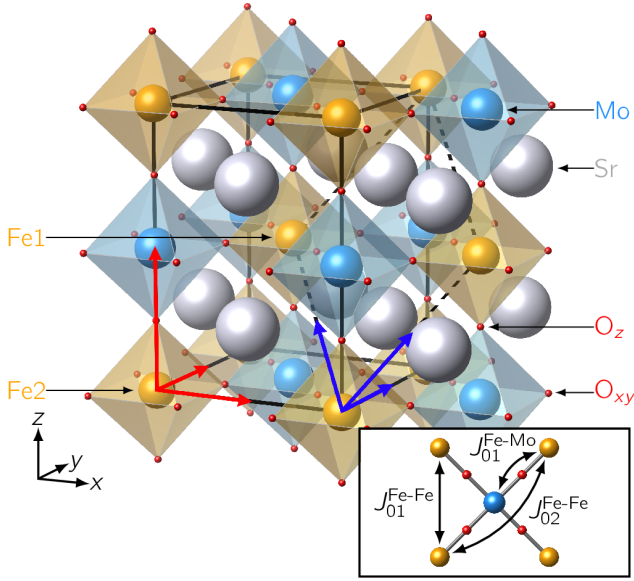


Figure 1. (Color online) The double perovskite structure of SFMO ($a = b = 5.573$ and $c = 7.902$ of Ref. [36]). The colored polyhedra visualize the octahedral surroundings of the Fe and Mo atoms (orange and blue). Following from the tetragonal symmetry, two different oxygen positions appear (marked with O_{xy} and O_z). The tetragonal supercell is shown by the black solid lines and the red arrows. It contains two functional units with two Fe sites (Fe1, Fe2). The black dashed lines and the blue arrows indicate the primitive unit cell. The inset shows the top view displaying the three most important magnetic coupling pairs between Fe-Fe and Fe-Mo. The figure was prepared with VESTA [39].

[35, 36]) or the oxygen octahedra are slightly distorted ($I4/m$, No. 87 [37, 38]). We used for simplicity the more symmetric body centered tetragonal structure type and the lattice constant and internal parameters from [36] as input for our study.

We note as well that the slight tetragonal distortion is lifting the degeneration of the d states. The crystal field at the Fe (Mo) site (now D_{4h} point symmetry) splits the Fe (Mo) $3d$ ($4d$) orbitals into three singlets A_{1g} (d_{3z^2}), B_{1g} ($d_{x^2-y^2}$), and B_{2g} (d_{xy}) and a doublet e_g (d_{yz} and d_{xz}). Since the deviation from the ideal c/a ratio is only small, the states d_{xy} and d_{3z^2} , as well as the states $d_{x^2-y^2}$, d_{yz} and d_{xz} , form two groups of states, which showed an almost similar density of states (DOS). Those are considered as e_g and t_{2g} in accordance with other publications.

For the microscopic understanding of the SFMO compound, we combined the theoretical results of three computational methods, namely the multiple scattering KKR-Green's function method HUTSEPOT [40, 41], the spin-polarized fully relativistic linear-muffin-tin-orbital (SPR-LMTO) method [42–44] and the Vienna *ab initio* simulation package (VASP) [45, 46]. The main investigation of the electronic and magnetic properties were conducted with HUTSEPOT, whereas the

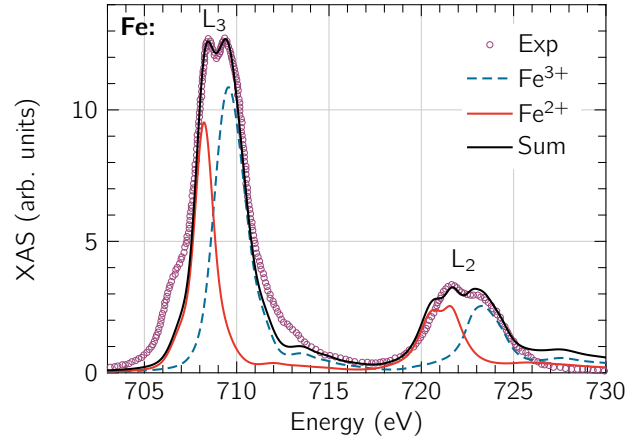


Figure 2. (Color online) The x-ray absorption spectra (Ref. [10], open circles) at Fe $L_{2,3}$ edges as average of left and right circularly polarized light in SFMO measured at 10 K with 5 T magnetic field compared with the theoretically calculated ones for Fe^{3+} (dashed blue line) and Fe^{2+} (solid red line). The linear combination of 60 % Fe^{3+} and 40 % Fe^{2+} denoted as Sum (solid black line) resembles best the reference curve.

XAS and XMCD spectra were calculated within the SPR-LMTO, and necessary structure relaxations were achieved with VASP. All relevant input parameters and the discussion about the correct treatment of the electronic structure of SFMO are provided in the Supporting Information (SI).

3. X-ray absorption and XMCD spectra

The valency of the Fe ions is not finally resolved. Experimental studies find a mixed valency state of Fe^{2+} and Fe^{3+} [6, 7, 10, 11] but theoretical calculations result a ground state with Fe^{3+} [23, 26, 47]. In order to solve this discrepancy, the x-ray absorption and XMCD spectra at the $L_{2,3}$ absorption edges can be used in a complex transition metal ionic compound such as SFMO as fingerprints of the ground state.

We used a supercell approximation with a cell of two functional units of SFMO (see red arrows in figure 1). This supercell was relaxed with VASP including a single oxygen vacancy close to Fe2. The relaxation with VASP for a single oxygen vacancy led to a distance of 1.9722 Å between Fe2 and the vacancy – an increase by 1.5 %. The correspondent distance between the Fe1 ion and the oxygen vacancy was reduced by 0.5 % to 4.4054 Å. In order to crosscheck effects of ASD on the calculated spectra, we included also one antisite defect into the supercell. We found, similarly as in [26], no significant internal relaxations.

The experimentally measured Fe $L_{2,3}$ absorption spectrum of the SFMO single crystal (Ref. [10], average of left and right circularly polarized light) displays at both absorption edges a weak lower-energy

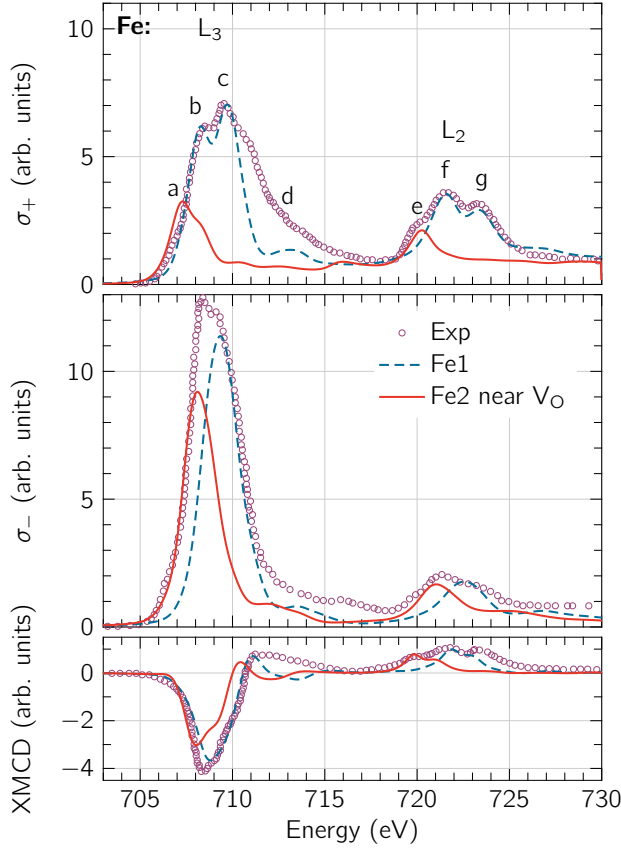


Figure 3. (Color online) The x-ray absorption spectra (Ref. [10], open circles) at Fe $L_{2,3}$ edges in SFMO measured with left (σ^+ , top panel) and right circularly polarized light (σ^- , middle panel) measured at 10 K with 5 T magnetic field and XMCD experimental spectrum (Ref. [10], lower panel) compared with the theoretically calculated spectra with an oxygen vacancy far away (dashed blue line) and near to an Fe ion (solid red line).

shoulder together with a doublet structure at the white line position with almost the same magnitude (figure 2). The complex fine structure of the Fe $L_{2,3}$ XAS is not compatible with a pure Fe^{3+} valency state, since we observed only one peak – similar to [13] – instead of a double peak structure. In order to provide a quantitative description of the spectral features, we took into account both Fe valencies $3+$ and $2+$, separately, using a primitive unit cell. The theoretically calculated Fe $L_{2,3}$ XAS agrees most closely with the experimental data by using those results in a linear combination of 60 % Fe^{3+} and 40 % Fe^{2+} (figure 2), which is opposite to the calculated proportion found in Ref. [10] using the framework of the ligand-field atomic formalism.

Considering that the correct Fe valency in the SFMO ground state is $3+$ as concluded in many theoretical studies, the mixed valency state might follow again from lattice defects as speculated in [13]. We investigated the influence of the two types of defects in the tetragonal supercell (figure 1). For the antisite

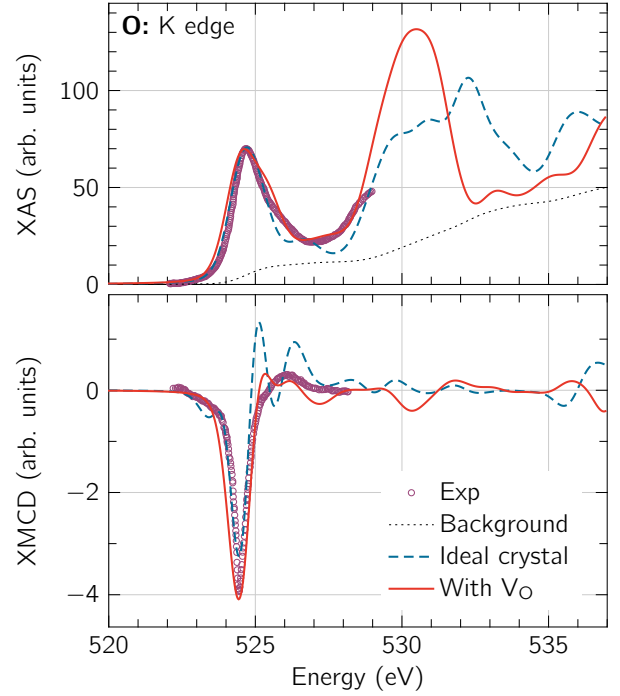


Figure 4. (Color online) The experimental x-ray absorption spectra (Ref. [12], open circles) at O K edge (top panel) in SFMO and experimental XMCD spectra (lower panel) measured at $T = 20\text{ K}$ with $B = 1.1\text{ T}$ compared with the theoretical simulations carried out for the ideal crystal structure (solid red line) and with an oxygen vacancy (dashed blue line).

defects, we observed only the Fe^{3+} solution. This can be connected with the high defect concentration modeled within the supercell. However, a single vacancy among twelve oxygen atoms models a more realistic concentration. Self-consistent calculations in the tetragonal supercell produce the valency of the Fe ions being equal to $2.9+$ and $2.4+$ at the Fe1 and Fe2 sites, respectively. Therefore, the existence of the vacancy shifts the valency of the nearest Fe ion (Fe2) towards $2+$. This valency change could be also observed below in the CPA calculation of the DOS including oxygen vacancies (figure 5).

Indeed, the full explanation of the experimental spectra is only possible by taking into account these crystal imperfections. The Fe L_3 x-ray absorption spectrum for left circularly polarized light (σ^+) possesses four major fine structures a , b , c and d (figure 3). We found that the calculations for the ideal crystal structure with the Fe^{3+} ground state solution (dashed blue line) provides the x-ray absorption intensity σ^+ only at the major peaks b , c , and d and do not reproduce the low energy shoulder (peak a) as well as the low energy peak e at the L_2 edge. The calculations with the Fe^{3+} solution produce only one high energy peak structure in the L_3 σ^- spectrum (middle panel). However, the experimental

measurements exhibit a double-peak structure. The x-ray absorption from the Fe2 atoms with the oxygen vacancy nearby (solid red line) contributes to the low energy peak of σ^- absorption (figure 3). The relative intensity of the peaks depends on the relative concentration of the Fe1 and Fe2 ions in SFMO, in other words, the concentration of defects such as oxygen vacancies. It is similar for the oxygen K edge. The calculations including an oxygen vacancy are in better agreement with the experimental measurements in the x-ray absorption as well as in the XMCD (figure 4).

The XAS and XMCD spectra at the Mo $L_{2,3}$ and $M_{2,3}$ edges are less sensitive for the crystal defects. For both edges the agreement with the experimental measurements [13] is quite good and independent from the concentration of oxygen vacancies (see SI, figures S4 and S5).

4. Electronic and Magnetic Properties with Randomly Distributed Oxygen Vacancies

We saw above that oxygen vacancies are certainly present in most samples of SFMO, while their impact on electronic and magnetic properties should be studied in detail. The KKR-GF method combined with the coherent potential approximation (CPA) allows the study of arbitrary concentrations of randomly distributed oxygen vacancies as done before for $\text{SrCoO}_{3-\delta}$ [33]. The oxygen vacancies were simulated inside the primitive unit cell with one functional unit of SFMO (see blue arrows in figure 1). The internal lattice positions had to be kept static [36]. We introduced a certain percentage of empty spheres at the lattice sites of the oxygen ions, which are modeled as randomly distributed via CPA. The typical oxygen-deficiency δ ranges between 0.006 to 0.36 [24, 29, 48]. This represents 0.1 at. % to 6 at. % of the total oxygen amount in defect-free SFMO.

We obtained for defect-free SFMO the half-metallic ground state by applying correlation corrections following Refs. [26, 47, 49] (figure 5). Although the half-metallic ground state would be well represented within the self-interaction correction (SIC) [47], the Fe d states localize too much. Hence, we applied an U parameter on the d states of Fe with $U_{\text{eff}}^{\text{Fe}} = 2 \text{ eV}$ as a compromise, because we are aware that the correct treatment of the electronic structure is very sensitive to the structural [23] and methodological differences [18, 28, 50] (see SI). Following optical [51] and photoemission spectroscopy (PES) [2–4] measurements, the band gap should be 0.5 eV to 1.3 eV, and should open between the Mo t_{2g}^{\uparrow} states and the Fe e_g^{\uparrow} states.

Of course, a direct comparison of calculated DOS and experimental spectra is very complicated, since

thermal broadening and defect levels can easily reduce the ideal band gap. Saitoh *et al* [2] noticed for example possible ASD in their samples (up to 10 at. %) but could not account for defects in their theoretical interpretation. ASD inside SFMO deteriorate the DOS at the Fermi energy E_F because new states appear in the majority spin channel [23, 25, 26, 28] and reduce the spin polarization, which was indeed observed experimentally [52]. In contrast, a low concentration of oxygen vacancies does not alter the half-metallic character of SFMO [25, 26, 30], but additional Fe d^{\downarrow} and Mo d^{\downarrow} states become occupied [26]. This indicates a lower valency of the Fe and Mo ions. Electrons of the removed oxygen atoms occupy states of Fe and Mo ions. A similar qualitative behavior was observed within our calculations of oxygen-deficient SFMO with CPA (green dashed line in figure 5). The averaging

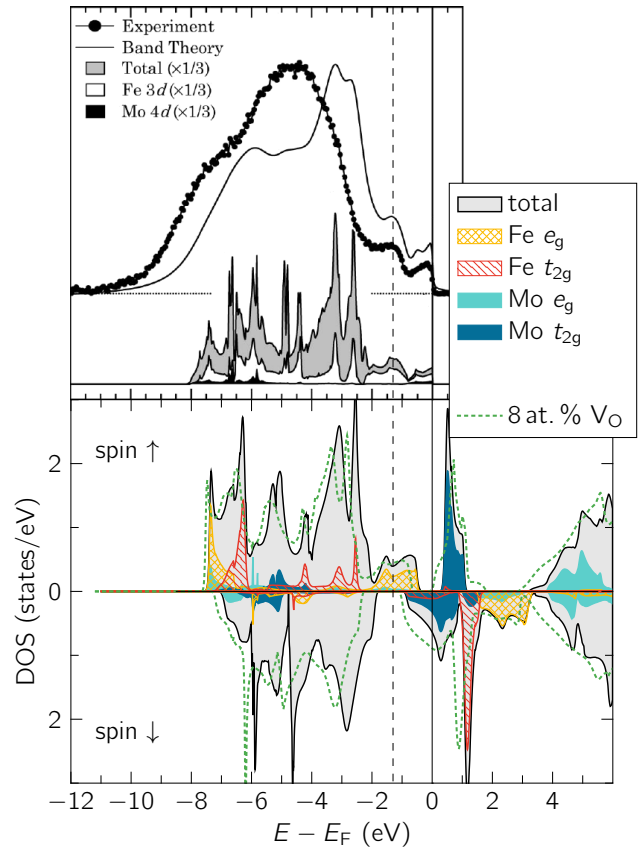


Figure 5. (Color online) The upper panel shows the experimental and simulated PES of SFMO taken as a copy of Fig. 5(a) of Ref. [2] (some labels were removed). The lower panel represents the DOS for SFMO calculated with the KKR-GF method and $U_{\text{eff}}^{\text{Fe}} = 2 \text{ eV}$. The gray area shows the total DOS for defect-free SFMO. The colored regions indicate the LDOS for the d states of Fe (reddish) and Mo (bluish). The green dotted DOS includes 8 at. % of randomly distributed oxygen vacancies. Both plots are scaled with respect to the same energy scale and the Fermi energy at zero (black vertical line). The dashed line indicates the position of the Fe e_g^{\uparrow} state in the experimental PES.

Table 1. The calculated spin m_s and orbital m_o magnetic moments (in μ_B) of Fe and Mo in defect-free SFMO compared with the measured magnetic moments. Experimental uncertainties are given in brackets behind the values.

method	Fe		Mo	
	m_s	m_o	m_s	m_o
SPR-LMTO	4.104	0.041	-0.504	0.047
KKR-GF	3.921		-0.525	
Ref. [10] ¹	3.05(20)	0.02(2)	-0.32(5)	-0.05(5)
Ref. [12] ¹	2.80(30)	0.093(10)	-0.36(3)	-0.037(15)
Ref. [8] ²	4.1(1)		0.0(1)	
Ref. [13] ³	3.72	0.042	-0.29	0.020
Ref. [53] ³	3.97		-0.39	

¹XMCD measurement

²Neutron diffraction experiment

³Theory

within the CPA broadens all states.

Even more interesting is the effect of oxygen vacancies on the magnetic properties of SFMO. As a starting point, we compare briefly the numerically obtained magnetic properties for defect-free SFMO with measured results and introduce then oxygen vacancies again. The expected ferrimagnetic (FiM) ground state of defect-free SFMO was always energetically favorable when comparing possible magnetic configurations. The Fe spin and orbital moments in FiM are parallel, whereas the spin and orbital Mo moments are antiparallel to each other, in accordance with Hund's third rule (table 1). We obtain a good agreement for the orbital Fe magnetic moment ($0.041 \mu_B$) with the FPLMTO result of Jeng and Guo [54] ($0.043 \mu_B$) and the LMTO results of Kanchana *et al* [13] ($0.042 \mu_B$). The calculated spin and orbital moments of the Mo atom are always larger in comparison with earlier calculations [13, 18, 53–55]. Also, the Fe spin moment of $\approx 4 \mu_B$ is in a good agreement with the experimental neutron diffraction measurements [8] and the theoretical ideal value for the $\text{Fe}^{3+}/\text{Mo}^{5+}$ or $\text{Fe}^{2+}/\text{Mo}^{6+}$ valency configuration (table 1). However, typical values for the magnetization reported in experimental studies are smaller than $\approx 4 \mu_B$. This reduction was always attributed to point defects [10, 22, 29, 56].

We used the CPA to simulate randomly distributed defects and indeed an almost linear decrease of the total magnetic moment agreeing qualitatively with an experimental study by Kircheisen *et al* [29] was observed (figure 6(b)). The offset of the measurement at $\delta = 0$ will result from other point defects like ASD [22]. Surprisingly, the Curie temperature is increasing with more oxygen vacancies, while the total magnetic moment is reduced at the same time (figure 6(b)). We obtained the Curie temperature T_C by calculation of the magnetic exchange interactions J_{ij} and consider them up to a distance of 12.49 \AA in a Monte Carlo simulation with a classical Heisenberg model [32]. These results

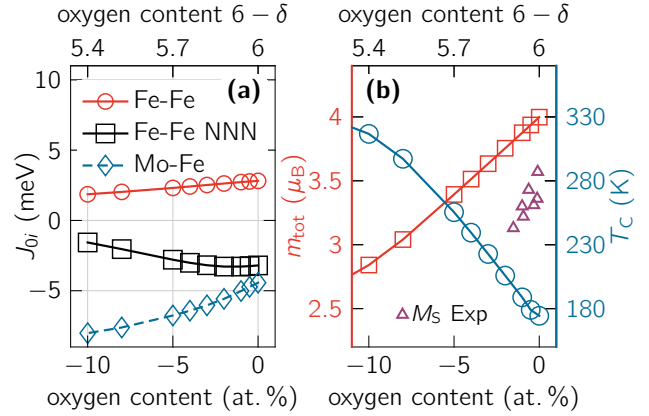


Figure 6. Calculated magnetic properties depending on the oxygen deficiency δ obtained with the KKR-GF method. (a) Magnetic exchange coupling constants for the strongest interactions (displayed in figure 1). (b) Total magnetic moment m_{tot} obtained within the self-consistent calculations and Curie temperatures from the Monte Carlo simulation. Experimental results [29] are given for the saturation magnetization (in μ_B).

agree also with the mean-field approximation (MFA) or the random-phase approximation (RPA) considering that MFA usually overestimates T_C .

Although T_C for defect-free SFMO is below the range of experimental values 324 K to 420 K, we are interested in the relative variation of T_C with the amount of oxygen vacancies, which is roughly +15 K per at. % of oxygen vacancies. Experimental results might therefore be enhanced by tens of kelvin due to oxygen vacancies.

The reasons for this increase in T_C can be understood from the magnetic exchange interactions. The most prominent coupling constants of the order of several meV have only a very restricted range up to 7.9 \AA (figure 6(a)). This includes only the interactions up to the next nearest neighbor Fe ions $J_{02}^{\text{Fe-Fe}}$ (see inset in figure 1). Due to the tetragonal structure, all magnetic exchange interactions show a small asymmetry with respect to those with a component in z direction. For clarity, only the coupling constants in the x - y -plane are shown (figure 6(a)).

The calculations of J_{ij} were performed in the FiM reference state. We observe for defect-free SFMO a strong antiferromagnetic (AFM) coupling between Fe and Mo ions and a ferromagnetic coupling between nearest neighbor Fe-Fe, $J_{01}^{\text{Fe-Fe}}$. The next nearest Fe-Fe coupling constants, $J_{02}^{\text{Fe-Fe}}$, have also an AFM character but are not enough to destabilize the FiM ground state of SFMO (see figure 6(a) for $\delta = 0$). Introducing now the oxygen mediated exchange between the Fe ions but favors the AFM exchange between Fe and Mo ions (figure 6(a)). This behavior resembles a stronger orbital localization as observed with an

increase of electron correlation parameter $U_{\text{eff}}^{\text{Fe}}$ (see SI). The stronger localization of the orbitals leads to a decrease of the electron hopping and, thereby, to a decrease in the magnetic coupling strength. Together, the total magnetic moment will be indeed reduced but the stronger AFM coupling between Fe and Mo sites will at the same time mediate an additional FM coupling and increases T_C .

5. Conclusions

We focused our study on the impact of oxygen defects on the magnetic properties of SFMO and made two crucial findings:

Our simulated x-ray absorption spectra (XAS) and x-ray magnetic circular dichroism spectra (XMCD) show a better agreement with experimental spectra [6, 7, 10, 11] than previous density functional calculations [13]. This indicates that the experimentally observed mixed valency of the Fe ion (Fe^{2+} or Fe^{3+}) is mainly caused by oxygen vacancies.

Second, we could explain the experimentally observed reduction of the total magnetic moment of SFMO by an increasing amount of oxygen vacancies following from a variation of the FM and AFM magnetic coupling between the Fe and Mo ions. At the same time, the Curie temperature shows a strong increase of roughly +15 K per at. % of oxygen vacancies.

Since the growing conditions of SFMO samples could be influenced by the oxygen partial pressure, oxygen vacancies could be a tool to improve the magnetic properties of SFMO, in particular, because the half-metallic band gap is not influenced by oxygen vacancies.

Acknowledgments

This publication was funded by the German Research Foundation within the Collaborative Research Centre 762 (projects A4 and B1). The support of the German Academic Exchange Service by grant “Electronic properties of thin SFMO films” (grant number 57071667) is greatly acknowledged.

References

- [1] Serrate D, De Teresa J M and Ibarra M R 2007 *J. Phys.: Condens. Matter* **19** 23201 URL <http://stacks.iop.org/0953-8984/19/i=2/a=023201?key=crossref.c682812d9d899d156577e366cddf1dbd>
- [2] Saitoh T, Nakatake M, Kakizaki A, Nakajima H, Morimoto O, Xu S, Moritomo Y, Hamada N and Aiura Y 2002 *Phys. Rev. B* **66** 035112 URL <http://link.aps.org/doi/10.1103/PhysRevB.66.035112>
- [3] Kang J S, Kim J H, Sekiyama A, Kasai S, Suga S, Han S W, Kim K H, Muro T, Saitoh Y, Hwang C, Olson C G, Park B J, Lee B W, Shim J H, Park J H and Min B I 2002 *Phys. Rev. B* **66** 113105 URL <http://link.aps.org/doi/10.1103/PhysRevB.66.113105>
- [4] Kim J H, Wi S C, Yoon S, Suh B J, Han S W, Kim K H, Sekiyama A, Kasai S, Suga S, Hwang C, Olson C G, Park B J, Lee B W and Introduction I 2003 *J. Korean Phys. Soc.* **43** 416
- [5] Sarma D D, Sampathkumaran E V, Ray S, Nagarajan R, Majumdar S, Kumar A, Nalini G and Guru Row T N 2000 *Solid State Commun.* **114** 465 URL <http://www.sciencedirect.com/science/article/pii/S003810980000079X>
- [6] Lindén J, Yamamoto T, Karppinen M, Yamauchi H and Pietari T 2000 *Appl. Phys. Lett.* **76** 2925 URL <http://scitation.aip.org/content/aip/journal/apl/76/20/10.1063/1.126518>
- [7] Kapusta Cz, Riedi P C, Zajac D, Sikora M, De Teresa J M, Morellon L and Ibarra M R 2002 *J. Magn. Magn. Mater.* **242-245** 701 URL <http://www.sciencedirect.com/science/article/pii/S0304885301009982>
- [8] García-Landa B, Ritter C, Ibarra M R, Blasco J, Algarabel P A, Mahendiran R and García J 1999 *Solid State Commun.* **110** 435 URL <http://www.sciencedirect.com/science/article/pii/S0038109899000794>
- [9] Moritomo Y, Xu S, Machida A, Akimoto T, Nishibori E, Takata M, Sakata M and Ohoyama K 2000 *J. Phys. Soc. Jpn.* **69** 1723 URL <http://journals.jps.jp/doi/abs/10.1143/JPSJ.69.1723>
- [10] Besse M, Cros V, Barthélémy A, Jaffrès H, Vogel J, Petroff F, Miron A, Tagliaferri A, Bencok P, Decorse P, Berthet P, Szotek Z, Temmerman W M, Dhesi S S, Brookes N B, Rogalev A and Fert A 2002 *Europhys. Lett.* **60** 608 URL <http://iopscience.iop.org/0295-5075/60/4/608/fulltext/>
- [11] Kuepper K, Balasz I, Hesse H, Winiarski A, Prince K C, Matteucci M, Wett D, Szargan R, Burzo E and Neumann M 2004 *Phys. Status Solidi A* **201** 3252 URL <http://doi.wiley.com/10.1002/pssa.200405432>
- [12] Koide T, Sekine T, Miyauchi H, Manaka H, Asakura D, Fujimori A, Kobayashi K I, Tomioka Y, Kimura T and Tokura Y 2014 *J. Phys.: Confer. Ser.* **502** 12003 URL <http://stacks.iop.org/1742-6596/502/i=1/a=012003?key=crossref.25c2e44b1ac9a2eaab026c4034ecf93d>
- [13] Kanchana V, Vaitheeswaran G, Alouani M and Delin A 2007 *Phys. Rev. B* **75** 220404 URL <http://link.aps.org/doi/10.1103/PhysRevB.75.220404>
- [14] Kato H, Okuda T, Okimoto Y, Tomioka Y, Oikawa K, Kamiyama T and Tokura Y 2004 *Phys. Rev. B* **69** 184412 URL <http://link.aps.org/doi/10.1103/PhysRevB.69.184412>
- [15] Rubi D, Navarro J, Fontcuberta J, Izquierdo M, Avila J and Asensio M 2006 *J. Phys. Chem. Solids* **67** 575 URL <http://www.sciencedirect.com/science/article/pii/S0022369705005561>
- [16] Paturi P, Metsänoja M and Huhtinen H 2011 *Thin Solid Films* **519** 8047 URL <http://dx.doi.org/10.1016/j.tsf.2011.06.059>
- [17] Saloaro M, Deniz H, Huhtinen H, Palonen H, Majumdar S and Paturi P 2015 *J. Phys.: Condens. Matter* **27** 386001 URL <http://stacks.iop.org/0953-8984/27/i=38/a=386001?key=crossref.b36a7568061928ddb9fd3377cbab54d2>
- [18] Kobayashi K I, Kimura T, Sawada H, Terakura K and Tokura Y 1998 *Nature* **395** 677 URL <http://www.nature.com/nature/journal/v395/n6703/pdf/395677a0.pdf>
- [19] Venimadhav A, Sher F, Attfield J and Blamire M 2004 *J. Magn. Magn. Mater.* **269** 101 URL [http://dx.doi.org/10.1016/S0304-8853\(03\)00570-5](http://dx.doi.org/10.1016/S0304-8853(03)00570-5) <http://linkinghub.elsevier.com/retrieve/pii/S0304885303005705>

- [20] Westerburg W, Reisinger D and Jakob G 2000 *Phys. Rev. B* **62** R767 URL <http://arxiv.org/abs/cond-mat/0001398><http://link.aps.org/doi/10.1103/PhysRevB.62.R767>
- [21] Kumar D and Kaur D 2010 *Physica B* **405** 3259 URL <http://www.sciencedirect.com/science/article/pii/S0921452610004254><http://linkinghub.elsevier.com/retrieve/pii/S0921452610004254>
- [22] Ogale A S, Ogale S B, Ramesh R and Venkatesan T 1999 *Appl. Phys. Lett.* **75** 537 URL <http://link.aip.org/link/APPLAB/v75/i4/p537/s1&Agg=doi>
- [23] Solov'yev I V 2002 *Phys. Rev. B* **65** 144446 URL <http://link.aps.org/doi/10.1103/PhysRevB.65.144446>
- [24] Colis S, Stoeffler D, Mény C, Fix T, Leuvrey C, Pourroy G, Dinia A, Panissod P and Meny C 2005 *J. Appl. Phys.* **98** 033905 URL <http://scitation.aip.org/content/aip/journal/jap/98/3/10.1063/1.1997286>
- [25] Stoeffler D and Colis S 2005 *J. Phys.: Condens. Matter* **17** 6415 URL <http://stacks.iop.org/0953-8984/17/i=41/a=012><http://stacks.iop.org/0953-8984/17/i=41/a=012?key=crossref.c42bbe9d47f773889dfdbfb0a0d4d6d>
- [26] Muñoz García A B, Pavone M and Carter E A 2011 *Chem. Mater.* **23** 4525 URL <http://dx.doi.org/10.1021/cm201799c>
- [27] Erten O, Meetei O N, Mukherjee A, Randeria M, Trivedi N and Woodward P 2011 *Phys. Rev. Lett.* **107** 257201 URL <http://link.aps.org/doi/10.1103/PhysRevLett.107.257201>
- [28] Reyes A M, Arredondo Y and Navarro O 2016 *J. Phys. Chem. C* **120** 4048 URL <http://pubs.acs.org/doi/abs/10.1021/acs.jpcc.6b00100>
- [29] Kircheisen R and Töpfer J 2012 *J. Solid State Chem.* **185** 76 URL <http://www.sciencedirect.com/science/article/pii/S0022459611005858>
- [30] Wu H, Ma Y, Qian Y, Kan E, Lu R, Liu Y, Tan W, Xiao C and Deng K 2014 *Solid State Commun.* **177** 57 URL <http://www.sciencedirect.com/science/article/pii/S0038109813004560>
- [31] Liechtenstein A I, Katsnelson M I, Antropov V P and Gubanov V A 1987 *J. Magn. Magn. Mater.* **67** 65 URL <http://www.sciencedirect.com/science/article/B6TJJ-46X4JHV-HX/2/a198d5cc2fb553863753292eb0284561>
- [32] Fischer G, Däne M, Ernst A, Bruno P, Lüders M, Szotek Z, Temmerman W M and Hergert W 2009 *Phys. Rev. B* **80** 014408 URL <http://link.aps.org/doi/10.1103/PhysRevB.80.014408>
- [33] Hoffmann M, Borisov V S, Ostanin S, Mertig I, Hergert W and Ernst A 2015 *Phys. Rev. B* **92** 094427 URL <http://journals.aps.org/prb/abstract/10.1103/PhysRevB.92.094427><http://link.aps.org/doi/10.1103/PhysRevB.92.094427>
- [34] Meneghini C, Ray S, Liscio F, Bardelli F, Mobilio S and Sarma D D 2009 *Phys. Rev. Lett.* **103** 046403
- [35] Park S I, Ryu H J, Kim S B, Lee B W and Kim C S 2004 *Physica B* **345** 99 URL <http://www.sciencedirect.com/science/article/pii/S0921452603010366>
- [36] Burzo E, Balasz I, Valeanu M and Pop I G 2011 *J. Alloys Comp.* **509** 105 URL <http://dx.doi.org/10.1016/j.jallcom.2010.08.126>
- [37] Nakamura S and Oikawa K 2003 *J. Phys. Soc. Jpn.* **72** 3123 URL <http://journals.jps.jp/doi/abs/10.1143/JPSJ.72.3123>
- [38] Azad A K, Eriksson S G, Khan A, Eriksson A and Tsegai M 2006 *J. Solid State Chem.* **179** 1303 URL <http://www.sciencedirect.com/science/article/pii/S0022459606000442>
- [39] Momma K and Izumi F 2011 *J. Appl. Crystallogr.* **44** 1272
- [40] Lüders M, Ernst A, Temmerman W M, Szotek Z and Durham P J 2001 *J. Phys.: Condens. Matter* **13** 8587 URL <http://stacks.iop.org/0953-8984/13/i=38/a=305>
- [41] Lüders M, Ernst A, Däne M, Szotek Z, Svane A, Ködderitzsch D, Hergert W, Györfy B L and Temmerman W M 2005 *Phys. Rev. B* **71** 205109 URL <http://link.aps.org/doi/10.1103/PhysRevB.71.205109>
- [42] Andersen O K 1975 *Phys. Rev. B* **12** 3060 URL <http://link.aps.org/doi/10.1103/PhysRevB.12.3060>
- [43] Nemoshkalenko V V, Krasovskii A E, Antonov V N, Antonov V I N, Fleck U, Wonn H and Ziesche P 1983 *Phys. Status Solidi B* **120** 283 URL <http://doi.wiley.com/10.1002/pssb.2221200130>
- [44] Antonov V N, Perlov A Ya, Shpak A P and Yaresko A N 1995 *J. Magn. Magn. Mater.* **146** 205 URL <http://linkinghub.elsevier.com/retrieve/pii/S0304885395010831>
- [45] Blöchl P E 1994 *Phys. Rev. B* **50** 17953 URL <http://link.aps.org/doi/10.1103/PhysRevB.50.17953>http://prb.aps.org/abstract/PRB/v50/i24/p17953_1
- [46] Kresse G and Joubert D 1999 *Phys. Rev. B* **59** 1758 URL <http://link.aps.org/doi/10.1103/PhysRevB.59.1758>
- [47] Szotek Z, Temmerman W M, Svane A, Petit L and Winter H 2003 *Phys. Rev. B* **68** 104411 URL <http://link.aps.org/doi/10.1103/PhysRevB.68.104411>
- [48] Yamamoto T, Liimatainen J, Lindén J, Karppinen M and Yamauchi H 2000 *J. Mater. Chem.* **10** 2342 URL <http://pubs.rsc.org/en/content/articlehtml/2000/jm/b003640>
- [49] Stoeffler D and Etz C 2006 *J. Phys.: Condens. Matter* **18** 11291
- [50] Sarma D D, Mahadevan P, Saha-Dasgupta T, Ray S and Kumar A 2000 *Phys. Rev. Lett.* **85** 2549 URL <http://link.aps.org/doi/10.1103/PhysRevLett.85.2549>
- [51] Tomioka Y, Okuda T, Okimoto Y, Kumai R, Kobayashi K I and Tokura Y 2000 *Phys. Rev. B* **61** 422 URL <http://link.aps.org/doi/10.1103/PhysRevB.61.422>http://prb.aps.org/abstract/PRB/v61/i1/p422_1
- [52] Panguluri R P, Xu S, Moritomo Y, Solov'yev I V and Nadgorny B 2009 *Appl. Phys. Lett.* **94** 012501 URL <http://scitation.aip.org/content/aip/journal/apl/94/1/10.1063/1.3058441>
- [53] Fang Z, Terakura K and Kanamori J 2001 *Phys. Rev. B* **63** 180407 URL <http://link.aps.org/doi/10.1103/PhysRevB.63.180407>
- [54] Jeng H T and Guo G Y 2003 *Phys. Rev. B* **67** 094438 URL <http://link.aps.org/doi/10.1103/PhysRevB.67.094438>
- [55] Saha-Dasgupta T and Sarma D D 2001 *Phys. Rev. B* **64** 064408 URL <http://link.aps.org/doi/10.1103/PhysRevB.64.064408>
- [56] Balcells L, Navarro J, Bibes M, Roig A, Martínez B and Fontcuberta J 2001 *Appl. Phys. Lett.* **78** 781 URL <http://scitation.aip.org/content/aip/journal/apl/78/6/10.1063/1.1346624>

Supporting information for:

Variation of magnetic properties of

$\text{Sr}_2\text{FeMoO}_6$ due to oxygen vacancies

Martin Hoffmann,^{*,†} Victor N. Antonov,^{‡,¶} Lev V. Bekenov,^{‡,§} Kalevi Kokko,^{||,⊥}
Wolfram Hergert,[#] and Arthur Ernst^{†,§}

[†]*Institute for Theoretical Physics, Johannes Kepler University Linz,
Altenberger Straße 69, 4040 Linz, Austria*

[‡]*G. V. Kurdyumov Institute for Metal Physics of the N.A.S. of Ukraine,
36 Vernadsky Street, 03142 Kiev, Ukraine*

[¶]*Faculty of Mathematics and Informatics, University of Bialystok,
K. Ciolkowskiego 1M, PL-15-245 Bialystok, Poland*

[§]*Max Planck Institute of Microstructure Physics, Weinberg 2, 06120 Halle, Germany*

^{||}*Department of Physics and Astronomy, University of Turku, FIN-20014 Turku, Finland*

[⊥]*Turku University Centre for Materials and Surfaces (MatSurf), Turku, Finland*

[#]*Institute of Physics, Martin Luther University Halle-Wittenberg,
Von-Seckendorff-Platz 1, 06120 Halle, Germany*

E-mail: martin.hoffmann@jku.at

Simulation of x-ray spectra

The x-ray absorption and dichroism spectra were calculated with the spin-polarized fully relativistic linear-muffin-tin-orbital (SPR-LMTO) method taking into account the exchange

splitting of the core levels. The approach for the x-ray absorption spectroscopy (XAS) and x-ray magnetic circular dichroism (XMCD) simulations is described in our previous papers.^{S1} The finite lifetime of a core hole was accounted for by folding the spectra with a Lorentzian. The widths of core level spectra $\Gamma_{L_2} = 1.14$ eV and $\Gamma_{L_3} = 0.41$ eV for Fe, $\Gamma_{L_2} = 1.83$ eV, $\Gamma_{L_3} = 1.69$ eV and $\Gamma_{M_{2,3}} = 2.1$ eV for Mo were taken from.^{S2} The finite apparative resolution of the spectrometer was accounted for by a Gaussian of width 0.6 eV.

In our SPR-LMTO simulations, the basis set consisted of the s , p , and d LMTO's for the Sr, Fe, Mo and O sites. The \mathbf{k} -space integrations were performed with the improved tetrahedron method [S3] and the self-consistent charge density was obtained with 1063 irreducible \mathbf{k} -points. We used a relativistic generalization of the LDA+ U method, which takes into account the spin-orbit coupling so that the occupation matrix of localized electrons becomes non-diagonal in spin indexes. This method is described in detail in our previous paper [S4] including the procedure to calculate the screened Coulomb U and exchange J integrals, as well as the Slater integrals F^2 , F^4 , and F^6 . The constrained LSDA calculations produce $J = 0.85$ eV for the Fe site in SFMO. In order to be consistent with the other methods, the Hubbard U has been used as an external parameter.

Table S1: The calculated spin m_s and orbital m_o magnetic moments (in μ_B) of Fe and Mo in defect-free SFMO compared with the LSDA+ U method (SPR-LMTO) and the results obtained via sum rules.

method	Fe		Mo	
	m_s	m_o	m_s	m_o
SPR-LMTO	4.104	0.041	-0.504	0.047
Sum rules	4.283	0.052	-0.464	0.041

Sum Rules We note that the spin and orbital magnetic moments were obtained from the XMCD experiments by using the sum rules, which relate the integrated signals over the spin-orbit split core edges of the circular dichroism to the ground state orbital and spin magnetic moments.^{S5} It is well known that the application of the sum rules sometimes results in an error up to 50 %.^{S6} To investigate the possible error of the sum rules in the case of SFMO we

compare the spin and orbital moments obtained from the theoretically calculated XAS and XMCD spectra through sum rules with directly calculated LSDA+ U values (table S1). The number of the transition metal 3d electrons is calculated by integrating the occupied d local density of states inside the corresponding atomic spheres, which gives the values $n_d^{\text{Fe}} = 6.737$ and $n_d^{\text{Mo}} = 4.552$. The sum rules reproduce the spin magnetic moments within 4 % and 8 % and the orbital moments within 21 % and 14 % for Fe and Mo, respectively (table S1).^{S7-S9}

XAS and XMCD for Mo Since the XAS and XMCD spectra were not influenced by the oxygen vacancies, we are here showing the obtained results for the L and M edge of the Mo ion for the sake of completeness (figures S1 and S2).

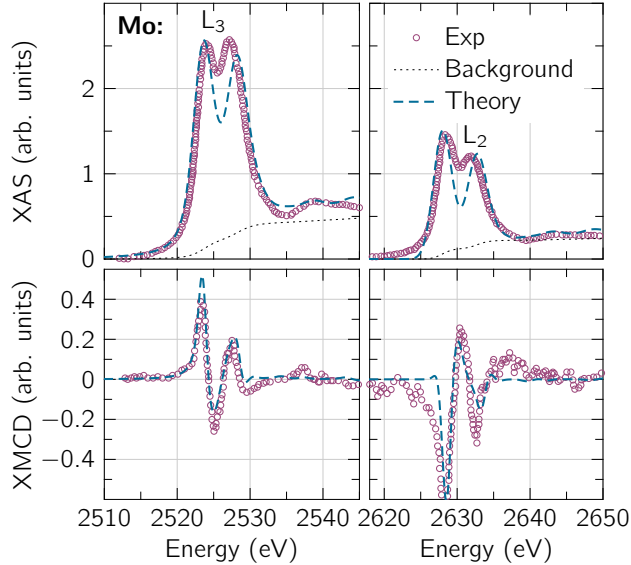


Figure S1: The experimental x-ray absorption spectra (Ref. [S10], open circles) at Mo $L_{2,3}$ edges (top panels) in SFMO measured at 10 K with 5 T magnetic field and experimental XMCD spectra (lower panels) compared with the theoretical simulations.

Electronic Structure

The orbital resolved density of states (DOS) was calculated with the Korringa-Kohn-Rostoker Green's function (KKR-GF) method called HUTSEPOT within the full-charge density approximation to the crystal potential. For the Green's function, the angular momentum cutoff

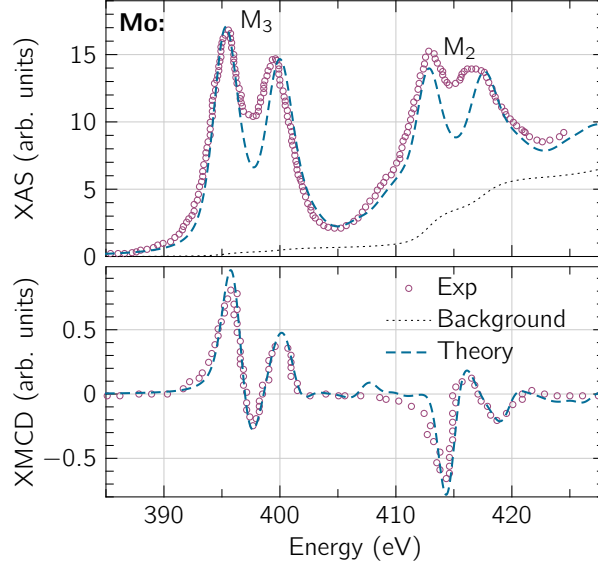


Figure S2: The experimental x-ray absorption spectra (Ref. [S11], open circles) at Mo $M_{2,3}$ edges (top panels) in SFMO and experimental XMCD spectra (lower panels) compared with the theoretical simulations.

was $l_{\max} = 3$ and the Brillouin zone integration was done with a \mathbf{k} -point mesh of $12 \times 12 \times 12$. The complex energy contour was integrated over 24 Gaussian quadrature points. With the Green's function $G(E)$ of the system, all quantities of interest follow in a straightforward way.

The exchange-correlation functional of a GGA-type was used very successful in the context of SFMO.^{S12,S13} Within the KKR-GF method, we used in particular the version of Perdew, Burke and Ernzerhof (PBE).^{S14,S15} In order to deal with the strong correlations in the oxide system, the GGA+ U approach of Dudarev *et al.* [S16] were used ($U_{\text{eff}} = U - J$).

We note, that the calculation of the electronic structure in SFMO is very sensitive to the choice of the atomic radii and the crystalline structure.^{S17} We used the atomic radii, obtained from the largest overlap of atomic potentials. Using smaller radii for the Fe atoms led to a half-metallic solution independent of the exchange-correlation functional – either LDA or GGA. We observed the same also within the SPR-LMTO method.

Half-metallic SFMO Although the half-metallic solution was previously obtained within the LDA and the GGA with different calculation techniques,^{S12,S19} the KKR-GF method

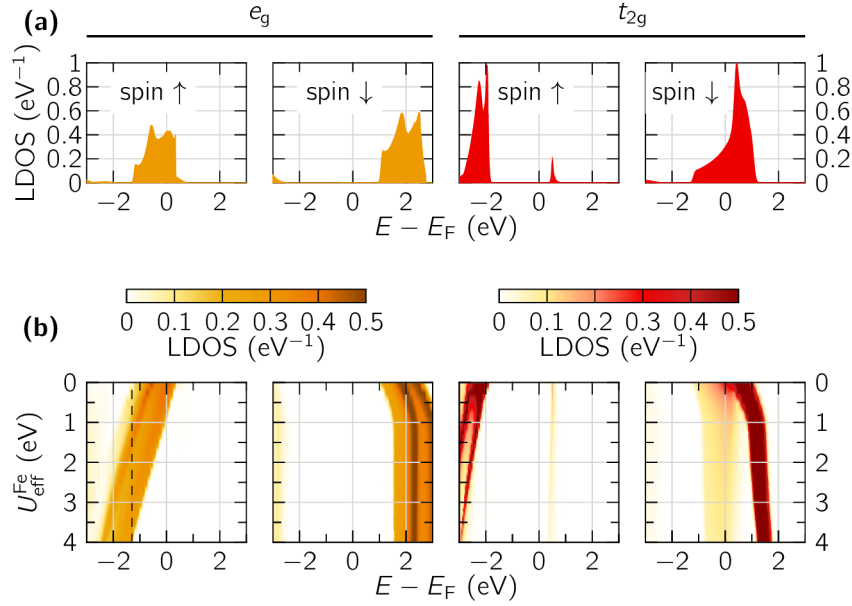


Figure S3: Atomic and orbital resolved DOS for the Fe d states: (a) GGA calculation and (b) GGA+ U . In (b) the DOS is color-coded as a contour plot. The dashed line in the left hand side panel indicates the peak position in the experimental PES. [S18](#)

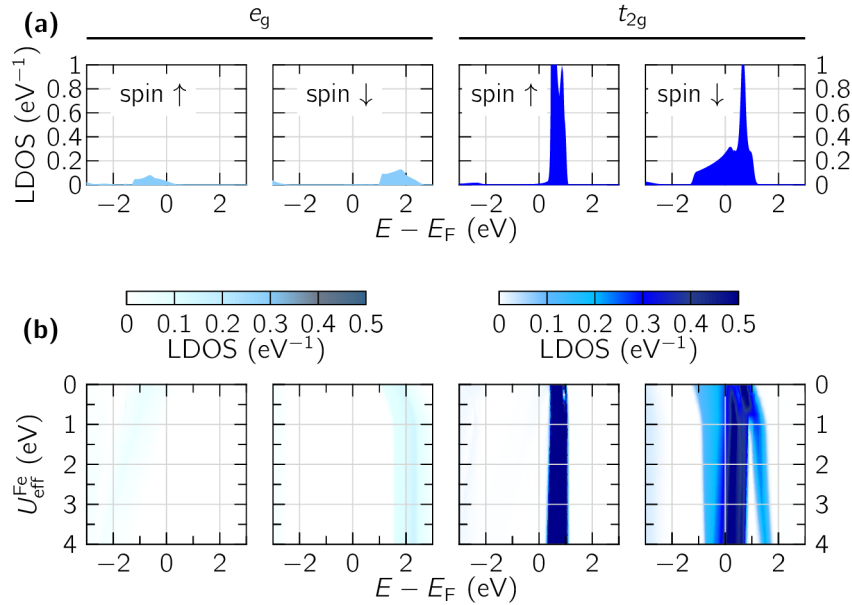


Figure S4: Atomic and orbital resolved DOS for the Mo d states: (a) GGA calculation and (b) GGA+ U . In (b) the DOS is color-coded as a contour plot.

yielded for the experimental lattice structure of Burzo *et al.* [S20] a metallic solution similar as in references [S21–S23] with a nonzero density of states in both spin channels at the Fermi energy, E_F , independent of the use of LSDA or GGA (for GGA see figures S3a and S4a). We also crosschecked the calculation of the DOS with the other methods and found similar results. The key point here seems to be the lattice structure, because small changes in the Fe-O and Mo-O bond length can influence the existence of the half-metallic band gap. S17

In order to obtain a better agreement for the Fe e_g^\uparrow state with the experimental observations, we calculated the DOS for several correlation parameters $U_{\text{eff}}^{\text{Fe}}$ applied only to Fe d states, and found a good agreement for $U_{\text{eff}}^{\text{Fe}} = 2 \text{ eV}$ (see dashed line in figure S3b). The main changes occur for the Fe e_g^\uparrow states at E_F , which crossed E_F for $U_{\text{eff}}^{\text{Fe}} \gtrsim 1 \text{ eV}$ and the band gap emerged. Then, almost all d^\uparrow (d^\downarrow) states of Fe are occupied (unoccupied), which is represented by a formal Fe^{3+} valence state. For the Mo ions, almost all states are unoccupied, except the delocalized t_{2g}^\downarrow states, which could be considered as a Mo^{5+} state. This situation was found in all self-consistent solutions with GGA+ U and represents the generally accepted ground state of SFMO. S12,S22,S24,S25 Thus, we use it as well in the description of the magnetic properties below.

Magnetic properties

We calculated the interatomic exchange coupling parameters J_{ij} from *ab initio* using the magnetic force theorem [S26] implemented within HUTSEPOT. The J_{ij} can be used in a Monte Carlo (MC) simulation to obtain the critical temperatures (details in references [S27–S29]). The convergence of the results concerning the number of MC steps, the cluster size, and the number of included J_{ij} was tested. We found that a cluster of $20 \times 20 \times 20$ unit cells is a good choice (figure 1 in the paper). We considered also periodic boundary conditions and restricted the calculation only to the magnetic atoms of the unit cell. The starting point was a high-temperature disordered state above the critical temperature T_C . In the course of

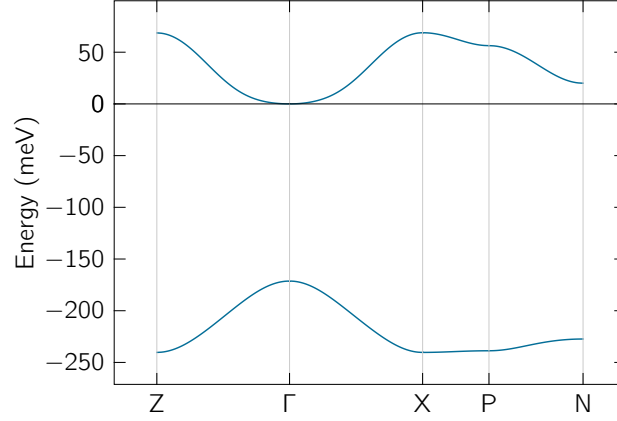


Figure S5: Magnon spectrum of half-metallic SFMO ($U_{\text{eff}}^{\text{Fe}} = 2 \text{ eV}$). The positive (negative) mode is associated mainly with the magnetic moments of Fe (Mo).

the simulations, the temperature was stepwise reduced until magnetic ordering was reached. For each temperature T , 20 000 MC steps are enough for the thermal equilibrium and the thermal averages were determined over 20 000 additional MC steps. T_C was then obtained from the temperature dependency of the magnetic susceptibility and the heat capacity within a numerical uncertainty range of $\pm 5 \text{ K}$. For comparison, T_C was also calculated with the mean-field approximation (MFA) and random-phase approximation (RPA).^{S30}

Magnetic ground state The underlying magnetic reference state for the calculation of the J_{ij} was the ferrimagnetic (FiM) solution – Fe moments align parallel to each other and Mo moments align antiparallel to the Fe moments. This was also identified as stable magnetic ground state by the calculation of the corresponding magnon spectrum (figure S5). The spectrum shows two well separated modes. In accordance with our analysis of the corresponding site-resolved magnonic Green function, the positive mode is mainly associated with the collective precession of Fe magnetic moments, while the negative mode reflects the properties of Mo magnetic moments. The different signs of the modes indicate on a ferrimagnetic ground state, which is confirmed by our total energy calculations.

However, Solovyev [S17] found that the FiM is not stable with respect to a spin spiral. The difference to our result might follow from our choice of taking the experimental lattice

structure of SFMO instead of the undisturbed cubic lattice structure.^{S17} Nevertheless, the FiM ground might be stabilized including breathing distortions of the oxygen octahedra. If the oxygen ion came closer to the Fe ions, the proposed spin spiral ordering became less favorable with respect to the FiM state but the half-metallicity was gone. These observations match ours. Our calculations within the GGA yielded for the experimental structure (where $d_{\text{Fe-O}}/d_{\text{Fe-Mo}} < 0.5$) a metallic ground state as well.^{S20}

References

- (S1) Antonov, V. N.; Yaresko, A. N.; Jepsen, O. *Phys. Rev. B* **2010**, *81*, 075209.
- (S2) Campbell, J. L.; Parr, T. *At. Data Nucl. Data Tables* **2001**, *77*, 1.
- (S3) Blöchl, P. E.; Jepsen, O.; Andersen, O. K. *Phys. Rev. B* **1994**, *49*, 16223.
- (S4) Yaresko, A. N.; Antonov, V. N.; Fulde, P. *Phys. Rev. B* **2003**, *67*, 155103.
- (S5) Ebert, H. *Rep. Prog. Phys.* **1996**, *59*, 1665.
- (S6) Antonov, V. N.; Jepsen, O.; Yaresko, A. N.; Shpak, A. P. *J. Appl. Phys.* **2006**, *100*, 43711.
- (S7) Ogale, A. S.; Ogale, S. B.; Ramesh, R.; Venkatesan, T. *Appl. Phys. Lett.* **1999**, *75*, 537.
- (S8) Balcells, L.; Navarro, J.; Bibes, M.; Roig, A.; Martínez, B.; Fontcuberta, J. *Appl. Phys. Lett.* **2001**, *78*, 781.
- (S9) Kirchseisen, R.; Töpfer, J. *J. Solid State Chem.* **2012**, *185*, 76.
- (S10) Besse, M.; Cros, V.; Barthélémy, A.; Jaffrès, H.; Vogel, J.; Petroff, F.; Mirone, A.; Tagliaferri, A.; Bencok, P.; Decorse, P.; Berthet, P.; Szotek, Z.; Temmerman, W. M.; Dhesi, S. S.; Brookes, N. B.; Rogalev, A.; Fert, A. *Europhys. Lett.* **2002**, *60*, 608.

- (S11) Song, J. H.; Jang, H. J.; Park, J.-H.; Jeong, Y. H. *IEEE Trans. Magn.* **2014**, *50*, 1001104.
- (S12) Kobayashi, K.-I.; Kimura, T.; Sawada, H.; Terakura, K.; Tokura, Y. *Nature* **1998**, *395*, 677.
- (S13) Xiang, H. P.; Wu, Z. J.; Meng, J. *Phys. Status Solidi B* **2005**, *242*, 1414.
- (S14) Perdew, J. P.; Burke, K.; Ernzerhof, M. *Phys. Rev. Lett.* **1996**, *77*, 3865.
- (S15) Perdew, J. P.; Burke, K.; Ernzerhof, M. *Phys. Rev. Lett.* **1997**, *78*, 1396.
- (S16) Dudarev, S. L.; Botton, G. A.; Savrasov, S. Y.; Humphreys, C. J.; Sutton, A. P. *Phys. Rev. B* **1998**, *57*, 1505.
- (S17) Solovyev, I. V. *Phys. Rev. B* **2002**, *65*, 144446.
- (S18) Saitoh, T.; Nakatake, M.; Kakizaki, A.; Nakajima, H.; Morimoto, O.; Xu, S.; Moritomo, Y.; Hamada, N.; Aiura, Y. *Phys. Rev. B* **2002**, *66*, 035112.
- (S19) Sarma, D. D.; Mahadevan, P.; Saha-Dasgupta, T.; Ray, S.; Kumar, A. *Phys. Rev. Lett.* **2000**, *85*, 2549.
- (S20) Burzo, E.; Balasz, I.; Valeanu, M.; Pop, I. G. *J. Alloys Comp.* **2011**, *509*, 105.
- (S21) Stoeffler, D.; Etz, C. *J. Phys.: Condens. Matter* **2006**, *18*, 11291.
- (S22) Muñoz García, A. B.; Pavone, M.; Carter, E. A. *Chem. Mater.* **2011**, *23*, 4525.
- (S23) Reyes, A. M.; Arredondo, Y.; Navarro, O. *J. Phys. Chem. C* **2016**, *120*, 4048.
- (S24) Szotek, Z.; Temmerman, W. M.; Svane, A.; Petit, L.; Winter, H. *Phys. Rev. B* **2003**, *68*, 104411.
- (S25) Erten, O.; Meetei, O. N.; Mukherjee, A.; Randeria, M.; Trivedi, N.; Woodward, P. *Phys. Rev. B* **2013**, *87*, 165105.

- (S26) Liechtenstein, A. I.; Katsnelson, M. I.; Antropov, V. P.; Gubanov, V. A. *J. Magn. Magn. Mater.* **1987**, *67*, 65.
- (S27) Fischer, G.; Däne, M.; Ernst, A.; Bruno, P.; Lüders, M.; Szotek, Z.; Temmerman, W. M.; Hergert, W. *Phys. Rev. B* **2009**, *80*, 014408.
- (S28) Otrokov, M. M.; Ernst, A.; Ostanin, S.; Fischer, G.; Buczek, P.; Sandratskii, L. M.; Hergert, W.; Mertig, I.; Kuznetsov, V. M.; Chulkov, E. V. *Phys. Rev. B* **2011**, *83*, 155203.
- (S29) Otrokov, M. M.; Ernst, A.; Tugushev, V. V.; Ostanin, S.; Buczek, P.; Sandratskii, L. M.; Fischer, G.; Hergert, W.; Mertig, I.; Kuznetsov, V. M.; Chulkov, E. V. *Phys. Rev. B* **2011**, *84*, 144431.
- (S30) Tyablikov, S. *Methods in the Quantum Theory of Magnetism*; Springer: Berlin Heidelberg, 1995.